

Fabrication of Microstructured Optical Fibres

Part II: Numerical Modelling of Steady-State Draw Process

S.C. Xue, R.I. Tanner, G.W. Barton, R. Lwin, M.C.J. Large and L. Poladian

Abstract — By combining theoretical, numerical and experimental analyses, this paper examines the continuous draw process that underpins fabrication of microstructured optical fibres (MOFs) with the aim of quantifying the impact of material properties and drawing conditions on the hole structure in the finished fibre.

Firstly by treating the continuous draw process as a steady-state, isothermal extensional flow of a Newtonian material, three-dimensional modelling clearly demonstrates how a combination of force effects can lead to dramatic hole deformation in the neck-down region – (i) surface tension contributing to hole size collapse (particularly if the fibre contains small holes and is drawn slowly over a long distance), while (ii) viscous effects are the major contributor to hole shape changes (particularly in cases where different size holes are in close proximity within the overall structure). Then the central role of the neck-down region in hole deformation is examined via non-isothermal numerical analysis. Results indicate that the shape of the neck-down region is highly sensitive to the viscosity profile and thus to temperature gradients. Finally it is shown that predicted hole deformations agree well with experimental measurements made in drawing polymethylmethacrylate (PMMA) MOFs.

I. INTRODUCTION

WITH the freedom provided by the ability to employ an almost limitless pattern of air holes, microstructured optical fibres (MOFs) have enormous potential in a diversity of applications from high-bandwidth telecommunications to precision sensing in astronomy [1].

However the optical properties implicit within the initial preform design may be significantly altered due to hole deformation (in both the size and shape of holes within the overall structure) during the fibre drawing processes. The impact of such deformation can be considerable particularly

for photonic bandgap fibres [2].

Previous theoretical analyses of the steady-state, isothermal drawing of an axisymmetric annular fibre allowed the prediction of hole size variations for such simple fibres [3, 4], the later study also considering shape changes for an isolated small hole located off-axis. However all such previous analyses were based on the assumed ‘slenderness’ of an extended preform or cane containing one single hole. To reliably predict hole deformation occurring within an arbitrary hole structure during fibre drawing requires detailed numerical modelling of the draw process.

In the first part of this study [1], we formulated the problem of drawing MOFs and to demonstrate the power of a numerical approach, the primary draw stage in our two-stage fabrication of microstructured polymer optical fibres (mPOFs) [5, 6] was simulated as a transient, isothermal process. Encouraging agreement was obtained with experimental data from mPOFs made from polymethylmethacrylate (PMMA).

In this second part, we report on numerical analysis and modelling together with experimental data for the continuous (secondary stage) draw process (see Fig.3 in [1]). Initially to focus our attention to (i) the impact of material properties and draw conditions on hole size changes, and (ii) the hole shape changes arising due to ‘interactions’ between the holes, the continuous draw process is treated as an isothermal deformation of a Newtonian material. Subsequent non-isothermal simulations focus on the influence of the drawing conditions on the shape of the neck-down region where most hole deformation occurs. Finally experimental data are given for mPOF containing various hole profiles. Note that the analysis and simulation results given here should be also readily applicable to MOFs made from any Newtonian material, such as silica [7].

II. ISOTHERMAL ANALYSIS AND SIMULATIONS

A. Hole collapse, enlargement and expansion

Hole size variation is a critical issue when drawing fibres containing holes, particularly if the anticipated final hole size is very small. In such cases holes may totally close (or collapse) due to surface tension effects when a preform (for silica MOFs) or cane (the intermediate stage in our mPOF fabrication process) is drawn to fibre.

Hole size variation due to drawdown can be investigated by considering the simplest geometrical configuration, that is, a

Manuscript received September 3, 2004. This work was financially supported by both the Australia Research Council and Cactus Fiber Pty Ltd. The support is gratefully acknowledged. All authors are from the University of Sydney, NSW 2006, Australia.

S. C. Xue and R. I. Tanner are with the School of Aerospace, Mechanical and Mechatronic Engineering, (email: shicheng@aeromech.usyd.edu.au; rit@aeromech.usyd.edu.au).

G. W. Barton and R. Lwin are with the Department of Chemical Engineering, (e-mail: barton@chem.eng.usyd.edu.au; R.Lwin@ofc.usyd.edu.au).

M. C. J. Large is with the Optical Fibre Technology Centre, (e-mail: MLarge@ofc.usyd.edu.au).

L. Poladian is with the School of Mathematics and Statistics, (e-mail: l.poladian@maths.usyd.edu.au).

single centrally located hole. To characterize hole size changes during the drawdown process, a collapse ratio C_o has been defined [3]:

$$C_o \equiv \frac{R_f(z)}{R_0(z)} / \chi. \quad (1)$$

Here (see Figs. 2 and 3 in [1]) $R_f(z)$ and $R_0(z)$ are the internal hole radius and the radius of a preform (or cane) at the axial position z , respectively. χ is the initial hole radius R_h relative to the initial radius R_i of the preform (i.e. $\chi \equiv R_h / R_i$).

With this definition, total hole collapse occurs when $C_o = 0$ (i.e. when $R_f = 0$), hole contraction occurs when $C_o < 1$, the status quo is preserved when $C_o = 1$, and hole expansion occurs when $C_o > 1$. Note that for the extending preform (or cane) to be characterized as a ‘slender body’, the aspect ratio ε must be very much less than 1. Here ε is defined as the ratio of R_i and the length over which the preform (or cane) is drawn down to fibre, i.e. $\varepsilon \equiv R_i/L$. The maximum extent of hole collapse at the draw exit ($z = L$) has previously been related to both the material properties and fibre drawing conditions [4],

$$C_o = 1 - \left(\frac{1}{\chi} \right) \left(\frac{1}{\ln D_r} \right) \left(\frac{1}{\varepsilon} \right) \left(\frac{1}{C_a} \right), \quad (2)$$

where the draw ratio $D_r \equiv V_f/V_i$ (i.e. the ratio of draw speed V_f to the feed rate V_i). The dimensionless group $C_a = \mu V_i / \sigma$ is called the capillary number and denotes the relative importance of viscous and surface tension forces. Here μ is the viscosity at a reference temperature while σ is the surface tension coefficient of the fibre material. From this relationship, we can see that small values of χ , ε and C_a , as well as D_r , all promote hole collapse.

However in practical fibre drawing, the extending preform or cane may not qualify as a slender-body. In these cases, in order to investigate hole size variations, numerical simulation is the only viable approach. A commercial software package called Polyflow [8] was used to carry out three-dimensional numerical simulations of the drawing of annular fibres. Two initial radius ratios (χ) and three aspect ratios (ε) were considered. Note that varying ε means that the fibres are drawn down from the same preform or cane but over different hot zone lengths. Figs. 1 and 2 show the results in terms of the collapse ratio C_o as a function of χ , ε and C_a . Clearly whether hole collapse ($C_o < 1$) or hole expansion ($C_o > 1$) occurs during the draw is determined not only by the magnitude of surface tension effects but also by the slenderness ε and the initial radius ratio χ .

It is also apparent that C_o approaches an asymptotic value (that varies with ε and χ) as C_a increases which indicates that surface tension effects can be ignored in this part of the drawing regime. However Eq. (2) shows that if surface tension is ignored but the slender body assumption is satisfied, then $C_o = 1$ which means that the inner hole and the preform (or cane)

will shrink together at the constant radial ratio at its initial value χ throughout the deformation length. However the aspect ratio range considered here ($\varepsilon = 0.125$ to 0.5) is clearly not low enough for the slender body approximation to hold, as the hole in the fibre is experiencing expansion ($C_o > 1$) even at high C_a values when surface tension should be negligibly important. Also we can see that if the slender body assumption is not applicable, then for a given aspect ratio a smaller hole leads to greater hole expansion, while for a given initial hole size, hole expansion is greater for a shorter neck-down region.

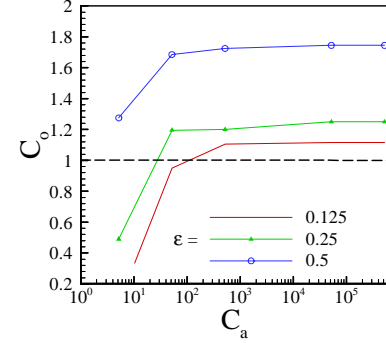


Fig. 1. Collapse ratio as a function of capillary number at different aspect ratios (ε) for an initial radius ratio $\chi=0.2$.

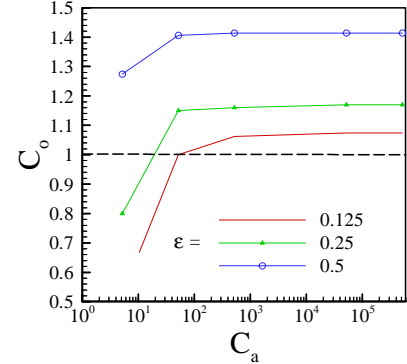


Fig. 2. Collapse ratio as a function of capillary number at different aspect ratios (ε) for an initial radius ratio $\chi=0.5$.

Numerical simulation reveals that hole expansion in the fibre is mainly due to an enlargement process experienced in the upper section of the neck-down region. Fig. 3 shows the hole boundary profile when drawing an annular fibre with $C_a = 520$ for the cases of (a) a small initial hole $\chi = 0.2$ drawn down over a short neck-down length ($\varepsilon = 0.5$), (b) a small initial hole ($\chi = 0.2$) drawn down over a long neck-down length ($\varepsilon = 0.125$), and (c) a large initial hole ($\chi = 0.5$) drawn down over a short neck-down length ($\varepsilon = 0.5$). As seen, for the cases of small initial hole, at the higher deformation rate ($\varepsilon = 0.5$) hole enlargement begins close to the start of the neck-down region. As a result considerable hole expansion ($C_o = 1.72$) is apparent in the final fibre. However no hole enlargement occurs at the lower deformation rate ($\varepsilon = 0.125$), and thus less hole expansion ($C_o = 1.2$) is apparent in this final fibre. Note that if the initial hole radius is increased to $\chi = 0.5$ under the same drawing conditions ($C_a = 520$ and $\varepsilon = 0.5$), then no hole

enlargement is predicted and the value of C_o for the final fibre reduces from 1.72 to 1.41. Therefore in the continuous draw process, the degree of hole enlargement experienced in the upper portion of the neck-down region is closely correlated with the extent of hole expansion in the final fibre. This phenomenon might well be exploited in minimizing hole collapse due to surface tension effects when drawing thin fibres containing small holes. Thus when drawing tapered MOFs [9], the approach taken should not only use a ‘fast and cold’ draw but the neck-down region should be as short as possible to encourage hole enlargement.

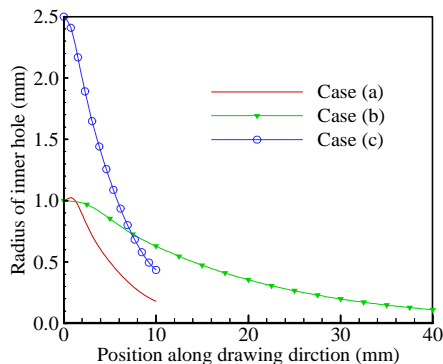


Fig. 3. Hole boundary profile along the drawing direction for an annular fibre drawn down with $C_a = 520$, (a) $\chi = 0.2$ and $\varepsilon = 0.5$, (b) $\chi = 0.2$ and $\varepsilon = 0.125$, and (c) $\chi = 0.5$ and $\varepsilon = 0.5$.

B. Hole shape changes

Next we considered shape changes arising from interaction between holes when drawing MOFs. The first case examined involves the drawdown of an intermediate cane with an initial radius R_i of 5 mm and a hole pattern as shown in Fig. 5, that is, a small hole ($\chi = 0.05$) centrally located with a larger hole ($\chi = 0.3$) located off-centre with the dimensionless (normalised against R_i) spacing between the two hole edges being $\Delta = 0.05$.

Fig. 4 also shows the shape of the neck-down region (left) and the cross-sectional hole pattern in the final fibre (right) drawn down from the intermediate cane using a 20 mm long hot-zone (i.e. $\varepsilon = 0.25$) at a relatively low draw ratio $D_r = 10$. As seen, a hole shape change similar to that predicted for the steep neck-down region in the primary stage of the mPOF draw process occurs [1], that is, the original circular small hole is deformed into an ovoid shape. Simulations with and without the inclusion of surface tension effects show no noticeable difference, indicating that surface tension is not responsible for this hole shape change. The shape changes become even more dramatic as the draw ratio is increased, as shown in Fig. 5. For a fixed length, a higher draw ratio means a ‘steeper’ neck-down region. Thus hole shape changes are closely related to the shape of the neck-down region.

Such dramatic shape changes are not simply the result of an asymmetrical hole pattern. This was clearly demonstrated in the first part of this study [1], where similar shape changes are observed for a pattern involving four symmetrically located

small holes. Indeed if we reverse the positions of the two holes in Figs. 4-5, a similar hole shape change is obtained, as shown in Fig. 6. Such hole shape changes can be characterized as a ‘curvature matching’ whereby the hole with a larger curvature (i.e. the smaller hole) changes its shape in such a way that the curvatures of any two adjacent holes tend to match each other. Thus the smaller hole tends to change its original circular shape to that of an ovoid with its major axis parallel to the surface of the larger hole.

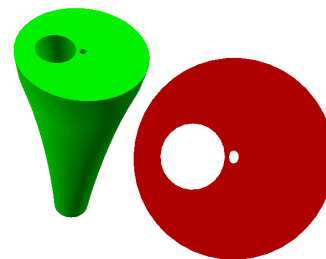


Fig. 4. Neck-down shape (left) and cross-sectional hole pattern (right) in a final fibre drawn at $D_r = 10$.

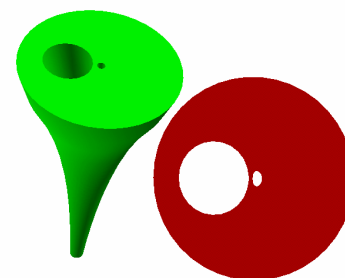


Fig. 5. Neck-down shape (left) and cross-sectional hole pattern (right) in a final fibre drawn at $D_r = 100$.

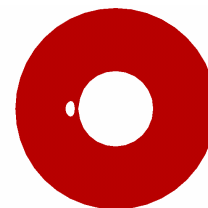


Fig. 6. Cross-sectional hole pattern in a final fibre drawn at $D_r = 100$.

For the case of two small holes of the same size with their spacing unchanged (i.e. $\Delta = 0.05$), the degree of hole shape deformation is greatly reduced (results not shown). Similarly if the spacing between the large and small holes shown in Figs. 4-6 is increased to $\Delta = 0.45$, the shape deformation is again greatly reduced (results not shown).

Thus for given drawing conditions, the extent of any shape change is influenced by the hole size, the spacing between holes, and the free surface boundaries in the vicinity of a hole. Numerical analysis indicates that dramatic hole shape changes are mainly due to the interaction between holes that are closely

adjacent but of different sizes. The greater the difference in size, the more dramatic are the expected hole shape changes. However if the holes are located too close to each other, then interaction can be such that the holes tend to merge with each other. This scenario is clearly demonstrated in Fig. 7 where we show the cross-sectional hole pattern in a fibre drawn down at $D_r = 150$ from a cane whose original hole pattern is shown on the top plane (left), that is, four circular holes with the same size ($\chi = 0.26$) symmetrically located around the central axis. The spacing between adjacent hole centres is here $\Delta = 0.424$.

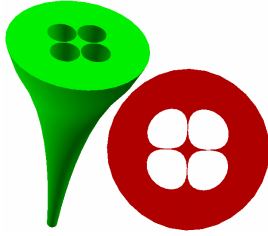


Fig. 7. Neck-down shape (left) and cross-sectional hole pattern (right) in the final fibre drawn at $D_r = 150$.

With regard to the observed ‘curvature matching’ feature, it should be noted that the hole shape change can be passed between neighbouring holes even if these all originally have the same size. This is demonstrated in Fig. 8 where we show the cross-sectional hole pattern in a final fibre drawn over a 20 mm long hot-zone at a draw ratio $D_r = 100$ from a cane whose original hole pattern is shown on the top plane (left). Here two additional small holes ($\chi = 0.05$) have been inserted alongside the original hole shown in Figs. 5 and 6 with the initial spacing between all adjacent hole surfaces kept at $\Delta = 0.05$. Due to the shape change of the centrally located small hole adjacent to the large hole, the other two small holes have also begun to change their shape so as to match their curvatures to that of their deforming neighbours.

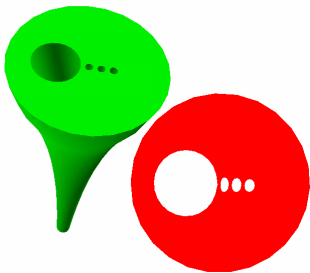


Fig. 8. Neck-down shape (left) and cross-sectional hole pattern (right) for a final fibre drawn at $D_r = 100$.

C. Approximate analysis of hole behaviour

Our numerical predictions have clearly demonstrated both hole size and shape changes. This behaviour seems decidedly more pronounced when the extending body (i.e. preform or cane) cannot be characterized as a ‘slender body’. The key questions here are (i) what causes the interaction(s) that lead to hole shape changes, and (ii) what are the driving forces that

lead to hole enlargement.

When drawing fibres containing holes, in the absence of surface tension and pressurization effects, with ignorable inertia, and gravitational forces, the only force involved is the draw tension force F . The driving forces causing hole size/shape changes must related to the force components induced inside the fibre body by F . In order to quantify these drivers, we need to carry out a localized force balance on the extending body.

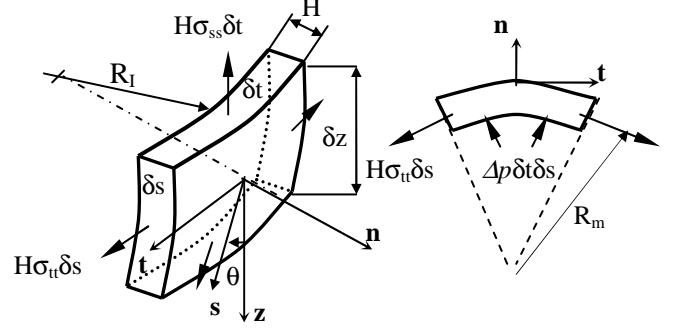


Fig. 9. Force balance on a localized finite volume fibre body.

Let us consider a finite volume $\delta s \times \delta t \times H$ sited between z and $z + \delta z$ (as shown in Fig.3 in [1]) in an extending annular body (i.e. either preform or cane). As shown in Fig. 9, δs , δt and H ($= R_o - R_i$) are the elemental dimensions in the meridional, tangential and normal directions under the intrinsic coordinates (n, s, t) located on the inner hole surface. θ is the angle between the z and s axes (i.e. the slope of the differential section). Let σ_{nn} be the average normal stress, σ_{tt} the average tangential (or hoop) stress, and σ_{ss} the average meridional stress – each component induced due to the drawing process. These stresses result in this finite volume extending in the drawing direction and shrinking in the radial direction. If an overpressure is applied within the hole, then a pressure difference Δp will clearly exist between the hole surface and the outer surface.

In force equilibrium during drawing, in the absence of surface tension effects a force balance in the n direction normal to the surface leads to the following,

$$\Delta p = H \sigma_{tt} K_m^t - H \sigma_{ss} K_m^s, \quad (3)$$

where K is the principal curvature (in the tangential or meridional directions as denoted by the superscripts t and s), while the subscript m denotes the middle point between the two surfaces. Thus,

$$K_m^t = \frac{\cos \theta_m}{R_m}; \text{ and } K_m^s = \frac{d^2 R_m}{dz^2} \cos^3 \theta_m, \quad (4)$$

with

$$\cos \theta_m = \frac{1}{\sqrt{1 + R_m'^2}}, \text{ and } R_m' = \frac{dR_m}{dz}. \quad (5)$$

In the absence of internal pressurization, Δp is zero, thus, from Eq. (3), we have

$$\sigma_{tt} = \left(\frac{K_m^s}{K_m^t} \right) \sigma_{ss}. \quad (6)$$

For an axisymmetric Newtonian flow, Eq. (6) can be cast as

$$-p + 2\mu \frac{u}{R_m} = \left(\frac{K_m^s}{K_m^t} \right) \sigma_{ss}. \quad (7)$$

or

$$u = \frac{R_m}{2\mu} \left(\frac{K_m^s}{K_m^t} \sigma_{ss} + p \right). \quad (8)$$

where p is the isotropic pressure, and u is the radial velocity on the middle plane. If $u > 0$, then, hole enlargement occurs.

By performing a force balance in the z direction, the meridional stress σ_{ss} can be obtained stress as

$$\sigma_{ss} = \frac{F}{2\pi R_m H \cos \theta_m}. \quad (9)$$

which is a tensile (positive) stress. Substitution of (4) and (9) into (8) gives:

$$u = \frac{R_m}{2\mu} \left(\frac{F}{2\pi H \sqrt{1+R_m^2}} \frac{d^2 R_m}{dz^2} + p \right) \quad (10)$$

From the analysis in drawing an annular hollow fibre in the absence of surface tension effects (see [4] for example), the leading-order solutions show that p is always negative and has a form as

$$p = -\frac{\mu v_z}{L} \ln D_r \quad (11)$$

with v_z being the extending filament's velocity in the drawing direction. So, the isotropic pressure always promotes fibre and hole contraction ($u < 0$), and a necessary (but not sufficient) condition for $u > 0$ is:

$$\frac{d^2 R_m}{dz^2} > 0. \quad (12)$$

that is, if, and only if the shape of the neck-down region is concave, is it possible for hole enlargement to occur. With a concave shape for the neck-down region, the meridional stress σ_{ss} induced by F will have a component acting outward. If this

component is larger than the component of the hoop stress σ_{tt} acting inward (as shown in Fig. 9), then material between the middle plane and the hole surface is pulled outward, while material between the middle plane and the outer surface is pushed inward so as to maintain mass conservation. As a result hole expansion/enlargement occurs.

From Eq. (10), we can see that for a given draw tension, hole enlargement is more likely to occur at that section where the slope of the neck-down is changing most dramatically (i.e. $|d^2 R_m / dz^2| \gg 1$). This point is usually located close to the entry plane ($z = 0$) where the isotropic pressure reaches the minimum if the leading order solution (i.e. Eq.(11)) is used to estimate p .

Hole expansion (or enlargement) can be one of the contributors to the interaction between holes in drawing MOFs, particularly when the holes are different sizes and in close proximity to each other. Differences in hole diameter mean that the driving forces moving material around the holes will vary with position. As a result, any small hole (for which there will be a smaller driving force due to the reduced area) in close proximity to a larger hole will find itself 'squeezed' and its shape altered. Such shape changes can be enhanced by both viscous and surface tension forces – the former being the most influential. We will show next that these viscous forces are inversely proportional to the hole radial dimensions.

The viscous force induced around a hole by draw tension in drawing fibre is the force that leads a hole to shrink together with the outer fibre in the absence of surface tension force. The magnitude of the viscous force around a centrally located hole can be estimated using the counterbalancing inner hole pressure force required to keep the hole radius unchanged (i.e. $dR_h/dz = 0$) whilst the perform (or cane) is shrinking in the radial direction (i.e. $dR_o/dz < 0$) throughout the neck-down region. From the force balance given by Eq. (3), we need to ascertain the induced hoop stress in terms of the localized deformation rates. By employing the geometrical similarity to the plastic 'film-blowing' process (see [10] for example), we use the result for the localized stress tensor for a Newtonian material in the absence of surface tension effects. The hoop stress reads (in our notation),

$$\sigma_{tt} = 2\mu v_z \left(\frac{1}{R_m} \frac{dR_m}{dz} - \frac{1}{H} \frac{dH}{dz} \right), \quad (13)$$

Note that here we have assumed that shear effects are not involved in the deformation process. However it is not necessary to assume that $H/R_o \ll 1$ (i.e. that we have a 'thin' film) but rather a constant value for the angle θ (see Fig. 9) which means that the slope of the neck-down region is constant (i.e. $|d^2 R_m / dz^2| = 0$) over the section. By substituting Eqs. (4) and (13) into Eq. (3), and rearranging we have:

$$\Delta p = \frac{2\mu v_z}{R_m \sqrt{1+R_m^2}} \left(R_o \frac{dR_l}{dz} - R_l \frac{dR_o}{dz} \right). \quad (14)$$

The viscous force F_{vis} around a hole is equal to the pressure force required to keep $dR_l/dz = 0$ (thus, $R_l = R_h$) throughout the section. Thus we have:

$$F_{vis} = \Delta p = \frac{8\mu v_s}{R_h \left(1 + \frac{R_o}{R_h}\right)^2 \sqrt{1+R_m^2}} \left| \frac{dR_o}{dz} \right|. \quad (15)$$

Thus not only is F_{vis} proportional to the local deformation slope within the neck-down region but also (like any surface tension force) is curvature dependent. The maximum value of this estimated viscous force will be at the draw exit where we require (at most) that $R_h = R_o$. Further at this point $\left| R_m' \right| \ll 1$ leading to the approximation:

$$F_{vis} \approx \frac{2\mu v_s}{R_h} \left| \frac{dR_o}{dz} \right|. \quad (16)$$

The dependence of F_{vis} on both the curvature of the hole and the slope of the neck-down region has important implications when drawing a fibre containing multiple holes with different diameters. In this case, we know that the surface tension forces around the various holes can be quite different due to the dependence of this force on hole radius. Thus one might expect shape changes due to interactions between holes arising from surface tension effects. However our present analysis indicates that the impact of the viscous force induced around a hole inside an extending body can be considerably more important, particularly if the neck-down region is steep. This fact can be clearly demonstrated by comparing F_{vis} with the surface tension force F_s acting around a hole,

$$F_s = \sigma K_l'. \quad (17)$$

and thus,

$$\frac{F_{vis}}{F_s} \approx 2 \left| \frac{dR_o}{dz} \right| C_a. \quad (18)$$

These forces ‘compete’ along the drawing direction with the ratio between the two not only characterized by the localized capillary number C_a but also dependent on the localized deformation rate. In that part of the neck-down region where the slope is steep, the viscous force will be dominant. However where the slope is less severe, the surface tension force may become important. But the fact that $C_a \gg 1$, particularly near the start of the neck-down region, means that it is the viscous force that is largely responsible for any hole shape changes. As a consequence one would expect it to be more difficult to maintain the original hole pattern if the fibre is drawn down using a short hot-zone. This conclusion has indeed been

confirmed by simulating the same fibre draw as shown in Fig. 5 but with the deformation length reduced to 10 mm (i.e. with ϵ increased from 0.25 to 0.5). Comparing Figs. 5 and 10 shows the expected more dramatic hole shape change in the latter case.

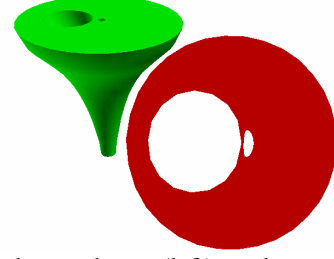


Fig. 10. Neck-down shape (left) and cross-sectional hole pattern (right) in the final fibre drawn at $D_r = 100$.

III. NON-ISOTHERMAL ANALYSIS AND SIMULATIONS

The isothermal analyses have clearly shown that the final hole structure within a MOF is strongly dependent on the shape of the neck-down region, and hence the viscosity profile along the extending body. In our continuous secondary mPOF draw process, the intermediate cane is gradually heated up – being preheated to about 110°C before it enters the hot-zone where it is further heated to the drawing temperature of about 185°C. Due to the strong dependence on temperature of the viscosity of fibre material (see, Eq. (9) in [1]), the viscosity can vary by several orders of magnitude in the draw direction. Clearly a non-isothermal simulation is necessary to achieve an accurate prediction of the neck-down shape, particularly in cases where the material used also has a low thermal conductivity (as does PMMA).

This section details non-isothermal numerical simulations performed for our secondary draw process. Emphasis is on the influence of operating conditions on the shape of the neck-down region, as this is now known to have a major effect on hole deformation. In our present draw tower, convective heat transfer dominates and thus here (as in the previous analysis [1]), radiative heat transfer is not considered.

Firstly, surface tension and viscous dissipation effects were investigated via three-dimensional simulations of the drawing of an annular hollow fibre from a 5 mm radius cane containing a concentric hole ($\chi = 0.25$). A constant temperature furnace ($T_h = 210^\circ\text{C}$) 50 mm in length was used, whilst the draw ratio D_r was set at 522. It was further assumed that the cane entered the hot-zone (after pre-heating) at 110°C whilst the convective heat transfer coefficient h in the hot-zone was constant at 10 $\text{W/m}^2\cdot^\circ\text{C}$. Thus for PMMA, the value of the Biot number (see [1], $B_i = hR_i / \kappa$) at the entrance plane was 0.25.

Fig. 11 shows the temperature distributions over the neck-down region calculated using Polyflow for two cases. Comparing Figs. 12(a) and 12(b) shows that the inclusion of surface tension and viscous dissipation has only a modest impact on the results, most notably a slight increase in fibre

temperature near the end of the draw-zone brought about by viscous dissipation together with a small amount of hole collapse ($C_o = 0.88$) due to surface tension.

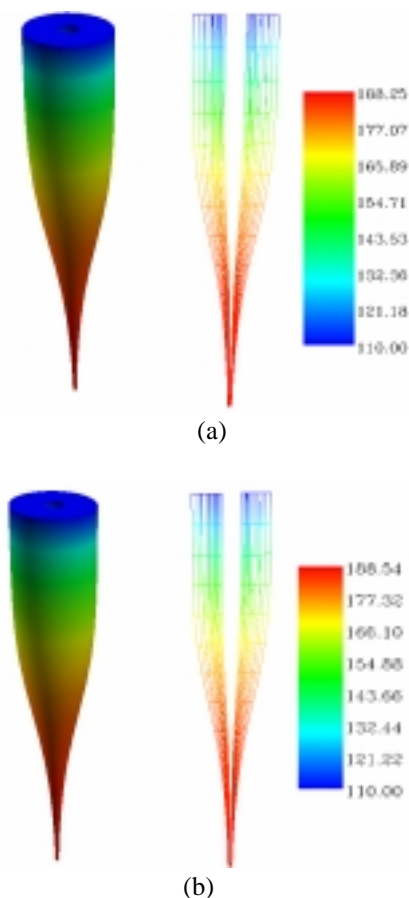


Fig. 11. Neck-down shape and temperature contour when drawing an annular PMMA fibre ($D_r = 522$ and $B_i = 0.25$). Surface tension and viscous dissipation effects are excluded in (a) but included in (b).

Next we considered the influence of operating conditions on the neck-down shape. To reduce the computational load, we only performed two-dimensional simulations of drawing solid fibres.

Fig. 12 shows the temperature profile (along both the fibre centre-line and at the external surface) for a solid fibre (treated as a Newtonian material) for five different values of B_i (0.01 to 1.0) corresponding to different h values (from 0.4 to 40 $\text{W/m}^2\cdot^\circ\text{C}$ for PMMA, for example). In each case D_r was fixed at 522. As expected the radial temperature difference (i.e. centre-line to surface) for a given axial position increases with B_i . However by the end of the hot-zone this radial temperature difference between cases had essentially disappeared. This is consistent with the fact that the local B_i has dropped to significantly below 0.1 by the end of the draw zone (see [1]) with the result that radial differences in temperature, viscosity and axial velocity at this point have effectively ceased to exist.

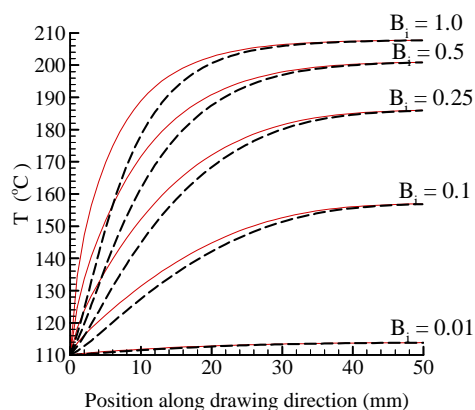


Fig. 12. Temperature profiles along solid fibre surface (solid lines) and fibre centreline (dotted lines) for different B_i values.

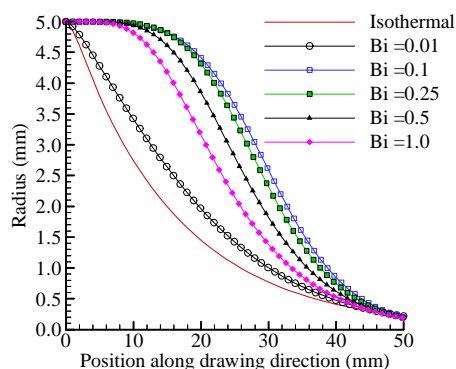


Fig. 13. Shape of neck-down region for a solid fibre drawn under isothermal and non-isothermal conditions.

The shape of the neck-down region under the same conditions as Fig. 12 are shown in Fig.13. Note that the isothermal case has been included for comparison. Clearly the external heat transfer coefficient (defined in terms of B_i) has a dramatic impact here. It is interesting to note that the onset of the neck-down region is delayed by increasing B_i between 0.01 to 0.1. However the onset of neck-down then starts earlier as B_i is increased between 0.1 to 1.0 although the shape is now starting with a convex, and ending with a concave rather than a concave throughout. An explanation for this behaviour is as follows. For a given draw at a fixed draw ratio (not draw tension), the profile of the neck-down region is purely determined by the relative (not absolute) value of viscosity along the axial (drawing) direction. The largest extensional deformation will occur at the position where viscosity reaches the lowest. Thus, for an isothermal simulation, the neck-down shape will be independent of the value of viscosity because of a constant temperature, and the extensional deformation starts immediately after the entry plane, and proceeds to the draw exit. However, for a non-isothermal draw, due to the temperature variation in the axial direction, dramatic variations in viscosity will occur. For the case of a very low Biot number (say $B_i \ll 0.1$), temperature is essentially uniform across any given cross-section. As a result viscosity, similar to what temperature does, is also essentially uniform across a cross-section (see Fig. 12 for $B_i = 0.01$) and the neck-down shape is

very similar to that of an isothermal draw (see Fig. 13 for $B_i = 0.01$). As Biot number increases (say $B_i \sim 0.1-1.0$), surface temperature changes more rapidly than the internal temperature with the result that a more pronounced radial difference occurs particularly in the upper portion of the neck-down region (see Fig. 12 for $B_i = 1.0$) where the radius is still relatively larger. However with rapid shrinkage in the external radius (which can be shown to be exponential for the isothermal drawing of a Newtonian ‘slender-body’), the local value of the Biot number rapidly decreases. As a result the cross-sectional temperature profiles in the axial direction become increasingly more uniform. The larger the value of the Biot number, the higher this ‘uniform’ temperature will be and the earlier this temperature is reached within the draw zone (see Fig. 12 for $B_i = 1.0$). Consequently extensional deformation (i.e. the onset of the neck-down region) starts earlier as predicted in Fig. 13.

For completeness we also investigated the impact of a non-uniform initial temperature profile T_i as the cane left the pre-heating section and entered the draw zone. The following radial (r) temperature profiles were considered,

$$T_i(r) = \frac{110 - C}{R_i} r + C, \quad (19)$$

with $C = 80, 100$ and 110 . The simulations (results not shown) indicated that such an inlet temperature profile had a minimal effect on the shape of the neck-down region.

From a fibre fabrication point of view, if the material, the furnace length, the cane and fibre diameters are all fixed, the only adjustable operating conditions relate to (i) the speed at which the cane is fed, (ii) the speed at which the fibre is drawn (or equivalently the draw ratio), and (iii) the temperature profile through the furnace.

By increasing the feed rate of the cane without adjusting (increasing) the draw ratio, the cane will stay within the furnace for a relatively shorter time, and as a result, its temperature will not rise as much if the heat transfer coefficient is kept the same. This qualitative line of reasoning is supported by the results shown in Fig. 14 which show the predicted axial temperature profiles for two cases where the feed rate differs by an order of magnitude. All other operating conditions are unchanged between cases (i.e. $D_r = 522$, $T_h = 210^\circ\text{C}$ and $h = 10 \text{ W/m}^2\cdot^\circ\text{C}$). Increasing the feed rate clearly impacts on both the shape of the axial temperature profile as well as the magnitude of the radial temperature profile at any given cross-section.

For a fixed draw ratio, the lower the cane feed rate (and thus a lower drawing speed), the higher the temperature that will be reached at a given position within the drawing fibre. However this does not mean that neck-down will start significantly earlier, as the cane will deform wherever its temperature is above the material softening point. More importantly what changes here with the feed rate is the draw force required to elongate the cane to fibre if the draw ratio is fixed. Fig. 15

shows the predicted neck-down region shape for the two cases given in Fig. 14 with the isothermal profile also given for comparison. For the lower feed rate, the temperature profile within the cane is such that the onset of significant neck-down is delayed (i.e. further away from the inlet plane) relative to that for the (10 times higher) feed rate. However the required draw force (which may be estimated via the axial stress for a uniaxial extensional flow) is substantially greater for the higher feed rate case as the viscosity is higher throughout the entire neck-down region. Here we need to emphasise that if the draw force is fixed, then totally different behaviour with respect to the onset of neck-down is to be expected if we change the feed rate.

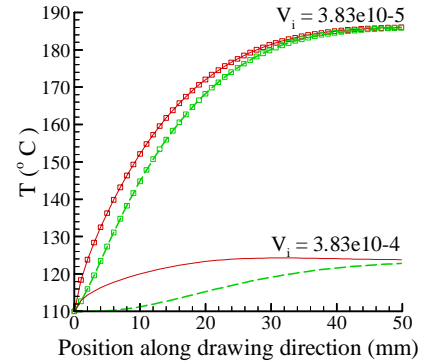


Fig. 14. Temperature profiles along solid fibre surface (solid lines) and fibre centre-line (dotted lines) for different feed speed, but fixed D_r .

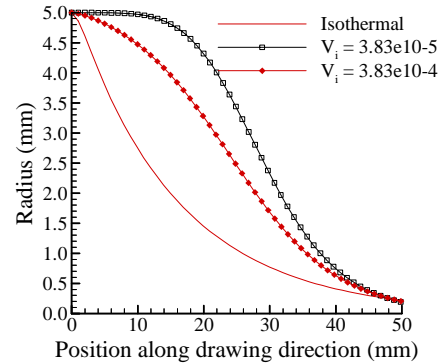


Fig. 15. Shapes of neck-down regions for solid fibres drawn under isothermal and non-isothermal conditions.

Thus far all simulations have assumed that the temperature within the furnace was constant. To quantify the impact of ‘heat leakage’ at the top and bottom of the furnace, the following heating temperature profile $T(z)$ was considered,

$$T(z) = \begin{cases} T_i + (T_h - T_i) z / L_1 & \text{for } 0 \leq z \leq L_1 \\ T_h & \text{for } L_1 \leq z \leq L_2 \\ T_h - (T_h - T_a) \frac{z - L_2}{L - L_2} & \text{for } L_2 \leq z \leq L \end{cases} \quad (20)$$

where T_i (the preheated cane temperature) is set to 110°C , T_h

(the wall furnace temperature) is set to 210°C, while T_a (the ambient temperature outside the furnace) is taken as 25°C. Values for L_1 (taken as 0.05L or 5% of the total furnace length) and L_2 (taken as 0.3L) were consistent with the measured temperature profile within our drawing furnace.

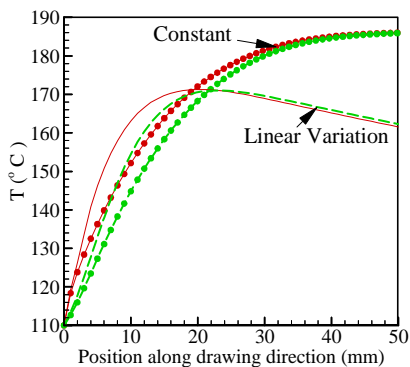


Fig.16. Temperature profiles along the fibre surface (solid lines) and fibre centre-line (dotted lines) for a solid PMMA fibre drawn under different furnace conditions.

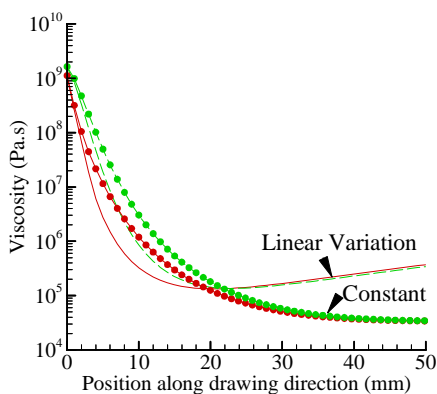


Fig. 17. Viscosity profiles along the surface (solid lines) and fibre centre-line (dotted lines) for a solid PMMA fibre drawn under different furnace conditions.

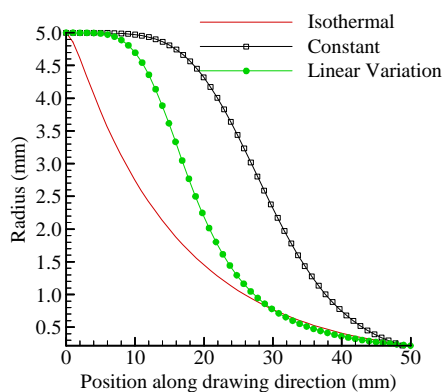


Fig. 18. Shape of neck-down region for a solid PMMA fibre drawn under different furnace conditions.

Fig. 16 compares the predicted temperature profiles for the cases where the furnace temperature is constant (at 210°C) and

varying with position. In both cases $D_r = 522$ and $B_i = 0.25$. Using Eq. (20) leads to a dramatic drop in fibre temperature in the lower portion of the furnace, with the result that viscosity here rises considerably. This is clearly shown in Fig. 17 with the outcome that there is a dramatic change in the shape of the neck-down region (see Fig. 18 where the isothermal profile is again included for comparison).

The two-dimensional non-isothermal simulations reported thus far have indicated that the mPOF secondary draw process is largely characterised by the importance of external heat transfer and the strong temperature dependence of PMMA's viscosity. Together these impact on the shape of the neck-down region which in turn affects the magnitude and form of any hole deformation. It should be noted that two related effects (not reported on here) can also impact on hole structure deformation. Non-uniform heat transfer in the circumferential direction would be expected to lead to asymmetric hole deformation. More importantly, polymers generally possess a stretch dependent viscosity (i.e. they can 'harden' as they are elongated), and it may be necessary to use a more complex rheological model to describe this type of behaviour [11]. Experimental data on the extent of PMMA's visco-elastic behaviour and the impact of its inclusion within POLYFLOW will be reported in a later paper.

IV. EXPERIMENTAL ANALYSIS

A. Hole enlargement, expansion and collapse

To quantify the extent of hole size deformation during the secondary draw process, PMMA annular fibres were drawn in a tower where convection is the dominant heat transfer mode. The canes used were 10-12 mm in diameter. In this draw tower, after the preheating section there is a 50 mm long hot-zone. Typically the cane begins to extend some 10-20 mm into the hot-zone depending on the efficiency of the heat transfer and the cane feed rate.

The measured variation of the collapse number and the radius of the inner hole relative to the initial hole radius are shown as functions of cane length in Figs. 19(a) and (b) for two cases where the initial hole radius ratio χ is substantially different (i.e. 0.037 and 0.22).

Focusing attention on the neck-down region, it can be seen that as the cane starts extending, the collapse number C_o increases considerably (above unity) in the upper portion of the neck-down region, indicating that hole expansion occurs here. Hole expansion is partially due to hole enlargement which is clearly shown in Fig. 19 (b) which demonstrates that the hole radius in the upper portion of the hot zone is larger than the initial hole radius. Maximal hole expansion has occurred by about the centre of the hot-zone. Further on, the collapse number falls as tapering to a final fibre continues and some measure of surface tension driven hole collapse takes place. By the time the fibre leaves the hot-zone, hole collapse has reached the stage where C_o has returned to unity (or indeed dropped below unity, particularly for the smaller hole case).

We note that as χ decreased, there was a greater degree of hole expansion – behaviour that is in agreement with our numerical simulations.

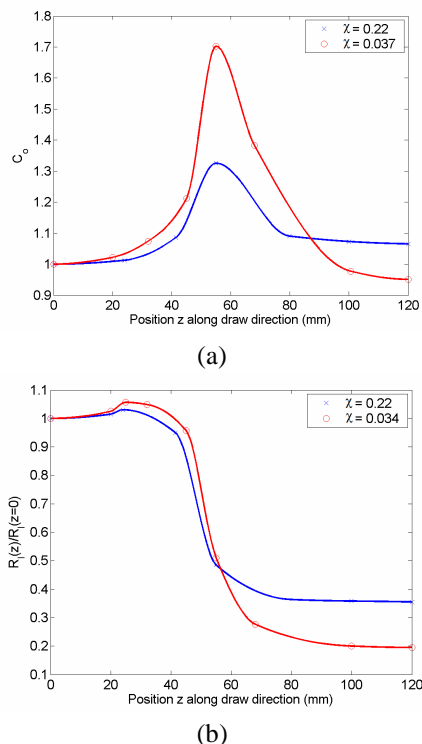


Fig. 19. Measured variation of (a) the collapse number and (b) the dimensionless hole radius for two PMMA annular fibres.

These results showed that while there is significant ‘hole activity’ in the neck-down region, surface tension only plays a significant role in the latter portion of this zone, with this effect becoming more pronounced as the hole size decreases.

B. Hole shape changes

Previously we reported on an experimental investigation of hole shape changes occurring in a five hole structure during the primary drawing of a PMMA preform (see Fig. 8 in [1]). These results showed that there were no dramatic hole shape changes in that part of the resultant cane away from the steep neck-down region near where the preform was supported.

These ‘good’ canes from the primary draw process were then drawn to fibre in our secondary draw tower. On average the cane radius was 5.34 mm, the dimensionless radius χ of the large hole and the four small holes was 0.202 and 0.039, respectively, while the dimensionless spacing between the centres of the large hole and a small hole was 1.96. Each cane was drawn to fibre at the same draw ratio ($D_r = 435$) with a feed rate of 2.3 mm/min.

Measurements at various cross-sections within the drawn fibre revealed that there were significant shape changes in the small holes (see also Fig. 8(b) in [1]). This effect can be partially attributed to these holes being located off-axis [3], but more importantly these shape changes are the result of the

interaction between holes with large size differences, as elucidated by the analysis and simulations reported earlier in the present study. As the deformed holes in the final fibre were ovoid in shape, the extent of deformation was quantified via the eccentricity e (where $e = 0$ for a circle and $0 < e < 1$ for an ellipse).

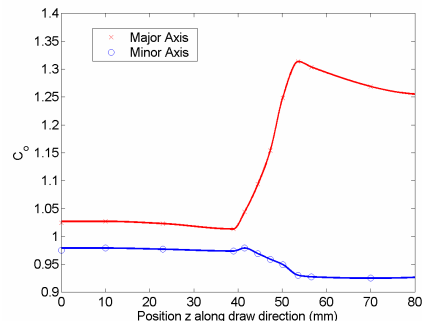


Fig. 20. Experimental values of the collapse number C_o for the small holes (for both major and minor axes).

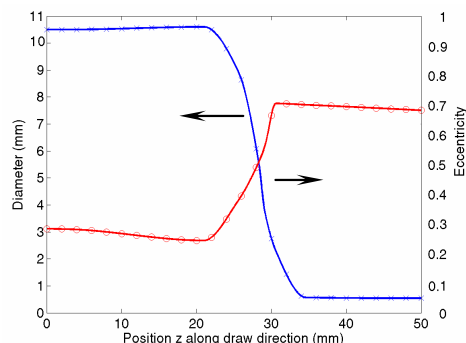


Fig. 21. Experimental profiles of the cane diameter and averaged small hole eccentricity along the hot-zone

Using values averaged over all four small holes, there were significant changes in each axis. Fig. 20 shows the variation in collapse number (for both axes) throughout the hot-zone. While the minor axis decreased by around 7% relative to its original circular value, the major axis experienced hole expansion that peaked at more than 30%.

Interestingly there was a significant difference between the results for the single centrally located hole case and this five-hole structure case. The former revealed that the relative size of the single hole ‘recovered’ to some extent in the latter portion of the hot-zone. However only a modest amount of recovery was seen in the latter portion of the hot-zone for the multi-hole case. These results clearly have major implications for any mPOF (such as a graded-index fibre) that contains a large number of holes covering a significant size range.

Fig. 21 shows the variation in both the outer diameter of the cane and the average eccentricity of the four small holes as the cane is drawn to fibre. It should be noted that the eccentricity of the small holes was already about 0.3 in the undrawn cane, due to shape deformation occurring in the primary draw stage. However the eccentricity of these holes more than doubled over the neck-down region in the secondary draw with little

‘recovery’ evident in the latter portion of this region.

To demonstrate ‘curvature matching’ in hole shape changes, experiments were also conducted by drawing PMMA fibres containing different hole structures. Fig. 22(a) shows clear evidence of the ‘curvature matching’ shape deformation expected for a fibre containing multiple holes of different diameters and in close proximity, while Fig. 22(b) shows evidence of how this curvature matching feature can ‘cascade’ through a series of holes even if they have the same size initially. This latter feature agrees well with the simulated results shown in Fig. 8.

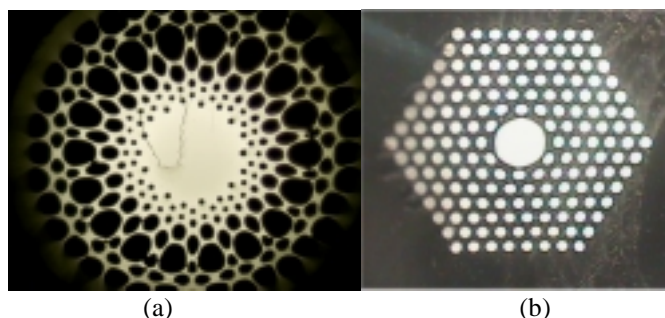


Fig.22. Cross-sections through (a) PMMA graded index MOF, and (b) photonic band gap mPOF.

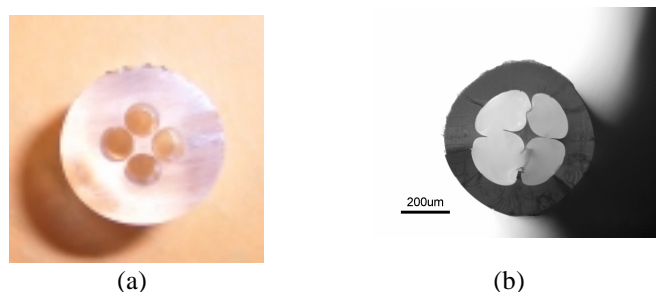


Fig. 23. PMMA suspended core fibre: (a) cane drawn from a preform with four closely spaced holes (see Fig. 8), and (b) final drawn fibre.

However when the holes are closely spaced, deformation can be observed even in cases where the holes are the same size, as previously demonstrated numerically (see Fig. 7). Experiments were also carried out for drawing the ‘suspended core’ hole structure shown in Fig. 7. Thus Fig. 23(a) shows the hole structure of the cane drawn from the preform in the primary draw stage, while Fig. 23(b) shows the hole structure of the final drawn fibre. As can be clearly seen, substantial shape deformation has occurred during the secondary draw (from cane to fibre), although minimal deformation is evident for the primary draw (from preform to cane) – observations that are in agreement with our numerical predictions.

V. CONCLUSIONS

A detailed investigation into hole deformation (in terms of both relative size and shape changes) is important for the

development of MOF technology. Whether a final fibre with a suitable hole pattern can be produced is strongly dependent on the interplay between the hole pattern design and the draw conditions. This study provides valuable guidance in this respect despite the fact that radiative heat transfer and non-Newtonian effects are still to be incorporated. These aspects are the focus of our on-going research.

The approach outlined here can be readily applied to any MOF provided that the relevant material and fabrication data are available.

REFERENCES

- [1] S. C. Xue, R. I. Tanner, G. Barton, R. Lwin, M. C. J. Large, and L. Poladian, “Fabrication of Microstructured Optical Fibres, Part I: Problem Formulation and Numerical Modelling of Transient Draw Process”, *J. Lightwave Technol.*, submitted, Aug. 2004.
- [2] N. A. Issa, M. A. van Eijkelenborg, G. Henry, M. Fellew, M. C. J. Large, “Fabrication and characterization of microstructured optical fibres with elliptical holes,” *Opt Lett*, vol. 29, pp. 1336-1338, 2004.
- [3] A. D. Fitt, K. Furusawa, T. M. Monro and C. P. Please, “Modeling the fabrication of hollow fibers: capillary drawing.” *J. Lightwave Technol.*, vol. 19, No. 12, pp.1924-1931, Dec. 2001.
- [4] S. C. Xue, R. I. Tanner, R. Lwin and G. Barton., “Drawing optical fibres containing holes,” *ZAMP*, to be submitted, 2005.
- [5] M. A. van Eijkelenborg, M. C. J. Large, A. Argyros, J. Zagari, S. Manos, N. A. Issa, I. Bassett, S. Fleming, R. C. McPhedran, C. M. de Sterke and N. A. P. Nicorovici, “Microstructured polymer optical fibre,” *Opt. Exp.*, vol. 9, No. 7, pp.319-327, Sep. 2001.
- [6] M. A. van Eijkelenborg, A. Argyros, G. Barton, I. Bassett, M. Fellew, G. Henry, N. A. Issa, M. C. J. Large, S. Manos, W. Padden, L. Poladian and J. Zagari., “Recent progress in microstructured polymer optical fibre fabrication and characterisation,” *Opt. Fiber Technol.*, vol. 9, pp.199-209, April. 2003.
- [7] J. C. Knight, T. A. Birks, R. F. Russell and D. M. Atkins, “All silica single-mode optical fiber with photonic crystal cladding,” *Opt. Lett.*, vol 21, No. 19, pp. 1547-1549, 1996.
- [8] POLYFLOW User’s Manual, ver. 3.10, Fluent Inc. Centerra Resource Park, 10 Cavendish Court, Lebanon, NH 03766,USA, Sep. 2003.
- [9] S. G. Leon-Saval, T. A. Birks, W. J. Wadsworth and P. St. J. Russell, “Supercontinuum generation in submicron fibre waveguides,” *Opt. Exp.*, vol. 12, No. 13, pp.2864-2869, June 2004.
- [10] J. R. A. Pearson and C. J. S. Petrie, “the Flow of a Tubular Film. Part 1. Formal Mathematical Representation,” *J. Fluid Mech.*, vol. 40, No.1, pp.609-625, 1970.
- [11] R.I Tanner, *Engineering Rheology*, (2nd Ed.), Oxford University Press Inc., New York, .2000.